



# Slab interactions in the Taiwan region based on the P- and S-velocity distributions in the upper mantle



Ivan Koulakov<sup>a,b,\*</sup>, Yih-Min Wu<sup>c</sup>, Hsin-Hua Huang<sup>c</sup>, Nikolay Dobretsov<sup>a,b</sup>, Andrey Jakovlev<sup>a</sup>, Irina Zabelina<sup>a,b</sup>, Kairly Jaxybulatov<sup>a,b</sup>, Viktor Chervov<sup>a</sup>

<sup>a</sup> Trofimuk Institute of Petroleum Geology and Geophysics, SB RAS, Novosibirsk, Russia

<sup>b</sup> Novosibirsk State University, Russia

<sup>c</sup> Department of Geosciences, National Taiwan University, Taipei, Taiwan

## ARTICLE INFO

### Article history:

Received 26 April 2013

Received in revised form 3 September 2013

Accepted 17 September 2013

Available online 1 October 2013

### Keywords:

Taiwan

Seismic tomography

Luzon arc

Ryukyu arc

Subduction

Collision

## ABSTRACT

We present a new model of P- and S-velocity anomalies in the upper mantle beneath the Taiwan region based on the inversion of travel time data from the global International Seismological Center (ISC) catalog. We clearly observed the anomalies of high P- and S-velocities associated with the subducting plates beneath the Ryukyu and Luzon arcs. At depths in the range of 100–200 km, the anomalies related to both slabs seem to be connected, which might be evidence of the lithosphere collision of the two oppositely oriented subduction zones. This model has been carefully verified using different synthetic tests. Based on the derived seismic model, we propose a model of recent plate reconstructions in the region around Taiwan. Initially, we presume the existence of two oppositely oriented subduction zones underneath the Luzon Island and the Ryukyu arc, separated with a transform fault. The NW movement of the Philippine Sea Plate led to first a shortening and then a disappearance of this transform fault. As a result, the edge of the Luzon arc collided with the edge of the Ryukyu arc. Simple simulations indicate that in this edge area, very strong stresses and deformation might take place that result in significant shortening of the earth surface. We believe that the origin of the Taiwan island was caused by the collisional processes due to the interaction of the two subduction zones. Note that in this case, no other conditions, such as the existence of arcs and/or buoyant continental crustal blocks, are required to explain the origin of the thick, strongly shortened crust in Taiwan.

© 2013 Elsevier Ltd. All rights reserved.

## 1. Introduction

The Taiwan area is greatly affected by active tectonic processes, which result in wide-spread seismicity and moderate volcanism. The 26 December 2006 Pingtung earthquake (Mw = 7.1 in the USGS catalog) and the historical records of seismicity had proved that the actively deforming accretionary wedge is capable of generating large, and most likely great, earthquakes. Recently, the USGS issued a report assessing the potential risk of a tsunami source occurring along the entire Pacific subduction zones and identified the Manila trench to the south of Taiwan as a high risk zone. For the safety of the highly populated Taiwan Island, the investigation of the nature of the tectonic activity is an important task to assess the seismic and volcanic hazard, which is impossible without robust knowledge on the deep structure of the crust and upper mantle.

As shown in Fig. 1, the Taiwanese tectonic activity is affected by a complex interaction of several major lithospheric plates. Being

located in a contact zone between the Eurasian and Philippine Sea plates, the tectonic processes in this area are mostly controlled by the relative kinematics of these two plates. In the east, the Philippine Sea plate subducts northward under the Eurasian plate along the Ryukyu trench. Off the southern tip of Taiwan, the South China Sea subplate, part of the Eurasian plate, subducts eastward under the Philippine Sea plate underneath the Luzon Island. The Taiwan Island is located at the junction between these two subduction zones (Fig. 2).

In addition, the other plates in the surrounding regions may contribute to the Taiwanese tectonic activity. The subduction of the Pacific Plate along the Izu-Bonin and Mariana arcs in some way affects the kinematics of the Philippine Sea Plate, which, in turn, determines the collision conditions in the Taiwan area. The role of the Indo-Australian Plate also appears to be important to tectonic activity in the region, as illustrated in Fig. 1B, which presents the simplified shapes of the main tectonic structures far outside the area of interest of this study. Some lineaments and blocks in this map are constructed based on the free-air gravity map by (Bonvalot et al., 2012) shown in Fig. 1A. The high-frequency gravity patterns in many cases are suitable for detecting hidden tectonic

\* Corresponding author at: Trofimuk Institute of Petroleum Geology and Geophysics, SB RAS, Novosibirsk, Russia. Tel.: +7 9134538987.

E-mail address: [KoulakovIY@ipgg.sbras.ru](mailto:KoulakovIY@ipgg.sbras.ru) (I. Koulakov).

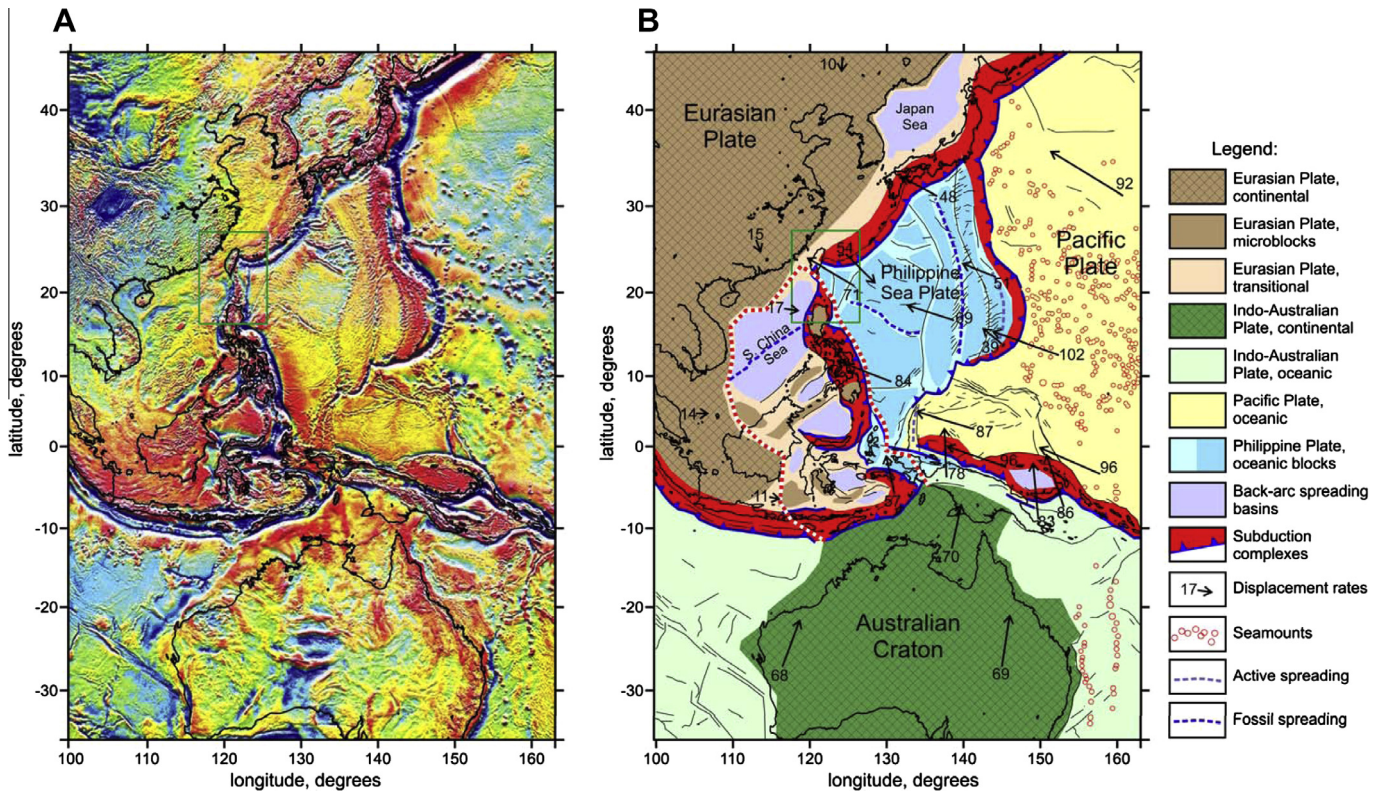


**Fig. 1.** Regional framework of the Taiwanese collision. (A) Free-air gravity map from (Bonvalot et al., 2012). (B) Simplified representation of the major tectonic structures. Black lines are the lineaments revealed from the gravity map. Displacement rates are given according to the global framework model by Bird (2003). Red dotted line indicates the area which is thought to be affected by collision with the Australian Craton. Green rectangle marks the study region. (For interpretation of the references to color in this figure legend, the reader is referred to the web version of this article.)

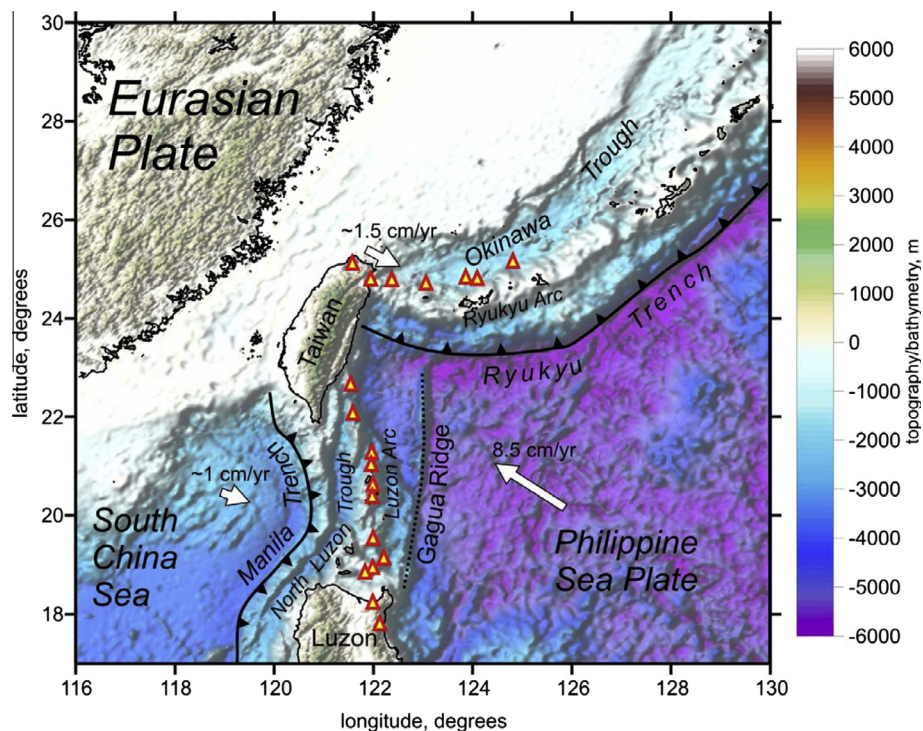


**Fig. 2.** Major tectonic elements in the study region. Background is the shaded topography/bathymetry map. Red triangles indicate recent volcanoes. (For interpretation of the references to color in this figure legend, the reader is referred to the web version of this article.)

structures under the sea bottom, which are not visible in bathymetry maps. The south-eastern part of Eurasia is observed to be composed of very heterogeneous lithospheric blocks of

continental and oceanic origin. In contrast to the Sunda arc, where the Indo-Australian oceanic plate forms the “classical” subduction zone, the collision of the Australian craton with the south-eastern

Asian margin causes strong deformations in the large area highlighted by the red dotted line in Fig. 1B. We believe that the Taiwan area, which is located at the northern edge of the deformed zone, might be affected by the northward displacement of the Australian indenter.

Taiwan is a place where exceptionally strong collisional processes occur, which led to the building of high mountains in a relatively small area. This mountain building is an indicator of active shortening, with a convergence rate of approximately 8 cm/years (Yu et al., 1997), which presumes strong compression forces in this region. The Taiwan orogeny, beginning at approximately 4 Ma (Suppe, 1984), is relatively young on the geological timescale. Several points of view exist on the origin of the collisional processes in the Taiwan region. Geologists have generally suggested that the orogen in the form of an accretion prism resulted from the eastward subduction of the Eurasian Plate, which is pulled beneath the Philippine Sea Plate by the subducted oceanic domain of the South China Sea (Suppe, 1981, 1984; Teng, 1990a,b; Malavieille et al., 2002). However, based on the local seismological observations, Wu et al. (1997) claimed that the orogen should be a result of lithospheric deformation caused by collision, not by subduction. Using the global seismic tomography image, Lallemand et al. (2001) illuminated the existence of the subducting South China Sea slab to be down to 670 km deep, with a possible slab detachment existing under the Coastal Range. The existence of this slab detachment is also favored in the continental exhumation model, where the slab serves a mechanism for the normal faulting of shallow earthquakes observed in the eastern Central Range (Lin, 2002). On the other hand, with regional magnetic and marine observations, Hsu and Sibuet (1995, 1997) proposed the arc-arc collision (Luzon arc and Ryukyu forearc) model in which the difference of the slab geometry in the upper mantle against that in previous models will be expected and needs to be examined in this study.

A question remains regarding the existence of a subduction zone directly beneath Taiwan: in the distribution of seismicity, we do not observe a clear Benioff zone, and previously published seismic tomography models do not provide unambiguous evidence of the slab beneath central Taiwan. In this sense, Taiwan is a particular place that requires additional geophysical investigations.

The deep seismic structure beneath the area of Taiwan has been actively studied by many authors during the last decades. One of the earlier tomographic studies in the Taiwan region was performed by Roecker et al. (1987) using the P-wave arrival times observed by the Taiwan Telemetered Seismographic Network (TTSN) consisting of only 25 stations. Later, the TTSN was incorporated into the Central Weather Bureau Seismic Network, which considerably increased the number of stations. The data of this larger network were used in several tomographic studies (e.g., Shin and Chen (1988), Rau and Wu (1995) and Ma et al. (1996)). More recently, Kim et al. (2005) conducted a tomography study for 3-D P- and S-wave velocity structures by jointly using data sets from the CWBSN and two temporary seismic arrays in Hualien and Pingtung. In a more recent studies by Wang et al. (2006, 2009), the arrival times from both local and teleseismic events were used to achieve a good resolution of the structures at greater depths. With a large number of earthquakes in and around Taiwan, the seismic velocity structures beneath Taiwan Island and the western part of the Ryukyu trench have been relatively well imaged through regional earthquake tomography (e.g., Hsu 2001; Kim et al. 2005; Lin et al. 2007; Wu et al. 2007; Ku and Hsu, 2009; Wang et al., 2008). In contrast, the offshore area of SW Taiwan, with the exception of some crustal-scale seismic profiles (Nakamura et al. 1998; McIntosh et al. 2005), is still poorly understood. The general configurations of the subducting plates in the study region are rather clearly seen in most global seismic models (e.g., Nakamura et al. 1998; Li et al., 2008).

Despite the existence of many studies, further continuation of the study of the deep structure beneath Taiwan is still important. In particular, some studies provide inconsistent and even contradictory features. Thus, additional work on validating the existing models is required to identify a robust and unambiguous solution.

Here, we present new regional tomography models in P- and S-velocities for the upper mantle beneath the Taiwan region, which is constructed based on the global travel time data. Although these models generally confirm previous findings, they provide important complementary material for the understanding of the slab configurations in the Taiwan region. In particular, the P- and S-models provide independent imaging for the same geological structures, and their correlation is an important argument for their verification. Based on the derived upper mantle structures, as well as on various available data, we propose a new plate reconstruction that explains the origin of the collisional deformations in the area of Taiwan.

## 2. Data and algorithm for the tomography inversion

For this study, we used the travel time data from the catalog of the International Seismological Center (ISC, 2001). All of the data in the ISC catalog have been reprocessed using the location algorithms described in Koulakov and Sobolev (2006). This algorithm includes a tool for the detection of outliers, which resulted in the rejection of almost 30% of the data. We defined the study region as a circle centered at 120° E and 24° N with a radius of 10°. The maximum depth in this study is 800 km. For this regional study, we used most of the data involving the ray paths that passed at least partially through the study volume. The data selected include (1) the data from the stations in the study region that record teleseismic events and (2) the data from earthquakes in the study area recorded by worldwide seismic stations (Fig. 3). For the first case, we used the information obtained by the 171 regional stations that recorded 212,000 P- and 68,000 S-rays from events located outside the circle. For the second case, the 13,267 events in the study area with the corresponding 916,000 P- and 296,000 S-rays recorded at all available epicentral distances were taken into consideration. The distributions of the earthquakes and the stations inside and outside the study area are displayed in Fig. 3. Satisfactory ray coverage is seen to only occur in a band along the subduction zone.

We used the tomographic algorithm that was initially presented in Koulakov et al., 2002 and then further developed by Koulakov and Sobolev (2006). This algorithm was successfully implemented for many regions, such as Europe (Koulakov et al., 2009), Asia (Koulakov, 2011), the Kurile-Kamchatka arc (Koulakov et al., 2011), and the Mariana and Izu-Bonin arcs (Jaxybulatov et al., 2013). The algorithm is based on a linearized one-step inversion. Any non-linear effects are thought to be minor and do not strongly affect the model. The travel times are corrected for the elevation of the stations, the ellipticity of the Earth and the crustal thickness.

The model is parameterized with a set of nodes distributed according to the ray density at some depth levels. For the Taiwanese region, we used the minimal grid spacing of 50 km for the map view. The grid was constructed on horizontal levels at depths ranging from 50 to 800 km and with a spacing of 50 km. The nodes were only installed in areas with sufficient ray coverage. The total number of nodes was 9876 and 9325 for the P- and S-models, respectively. To avoid any effect of the basic grid orientation and to make the solution less grid dependent, we performed the inversion for two irregular grids with different predefined orientations at 0° and 45°. After computing the results for these two cases, they are averaged and recalculated in a single model.

The inversion is performed simultaneously for the P- and S-velocity models, the source parameters, and the station corrections. For the teleseismic events, we used only one unknown parameter per source (the shift of the origin time), whereas for the regional case, four parameters (the three coordinates and the origin times) were determined for each event. The inversion of the large sparse matrix was performed using the LSQR algorithm (Paige and Saunders, 1982; Nolet, 1987). We used two types of damping, namely amplitude regularization with the diagonal unit matrix and smoothing, which minimizes the differences in the solutions for all combinations of the neighboring nodes in the grid. The optimal values of the parameters for the grid construction and inversion were determined by synthetic modeling (see the next section). Note that the parameterization grid spacing is significantly smaller than the resolved capacity of the model. We control the resolution by the tuning the damping coefficients so that any valuable anomaly was based on several nodes (4–6). In this case changing the grid spacing, rotations or displacements of the grid would not cause any change in the result. In this sense, such parameterization can be considered as quasi continuous.

### 3. Inversion results and verification

The variance reduction of the time residuals after one iteration step of the tomographic inversion was approximately 56%. Such a relatively large variance reduction is explained by the existence of high-amplitude patterns in the mantle related to the subducting plate, which were successfully retrieved by the tomographic inversion.

The results of the inversion for the P- and S-anomalies are shown in the horizontal (Figs. 4 and 5) and the two vertical sections (Figs. 6 and 7). At first sight, we should emphasize a rather

clear correlation between the P- and S-models, which seem to display the same structures. The most prominent feature in both models is the high-velocity linear patterns, which are associated with the subducting Philippine Sea Plate beneath the Ryukyu arc and the Eurasian Plate beneath the Luzon arc. The presence of these slab segments is supported by the distribution of the Benioff seismicity and the previous regional and global tomography studies (e.g., Rau and Wu, 1995; Bijwaard et al., 1998; Lallemant et al., 2001; Wang et al., 2006; Wu et al., 2007).

At a depth of 50 km, the uppermost section exhibits integral values of the velocity anomalies in the crust and the uppermost mantle. At this depth level, the P- and S-anomalies are almost perfectly coherent. The strongest negative anomalies are observed beneath Taiwan and the Luzon Islands, where the continental type of the crust is presumed by most authors (e.g., Lin, 2000; Chemenda et al., 2001). Strong negative anomalies are also observed beneath the volcanic islands along the Ryukyu and Luzon volcanic arcs. The high P- and S-velocities at the shallowest level are observed beneath the oceanic regions, where the crust is thought to be thin. The difference between these low- and high-velocity patterns is especially sharp for the S-model. The P-model reveals some structures in the ocean as low-velocity patterns, such as the Gagua Ridge, whereas the S-model attributes the high velocities to most of the oceanic areas.

At a depth of 150 km, the slab-related anomaly is most clear and consistent for the P- and S-models. In both models, this anomaly follows the Ryukyu arc, then makes a loop beneath the Taiwan Island and jumps to the Luzon arc. Note that at this depth, the Ryukyu and Luzon slab-related anomalies have the appearance of connected patterns. For the depths of 250 km and 350 km, we observe a clear gap between these anomalies in the P-model. In the S-model, this gap is less clear, which can be explained by the significantly smaller amount of the S-data that provide the information at this

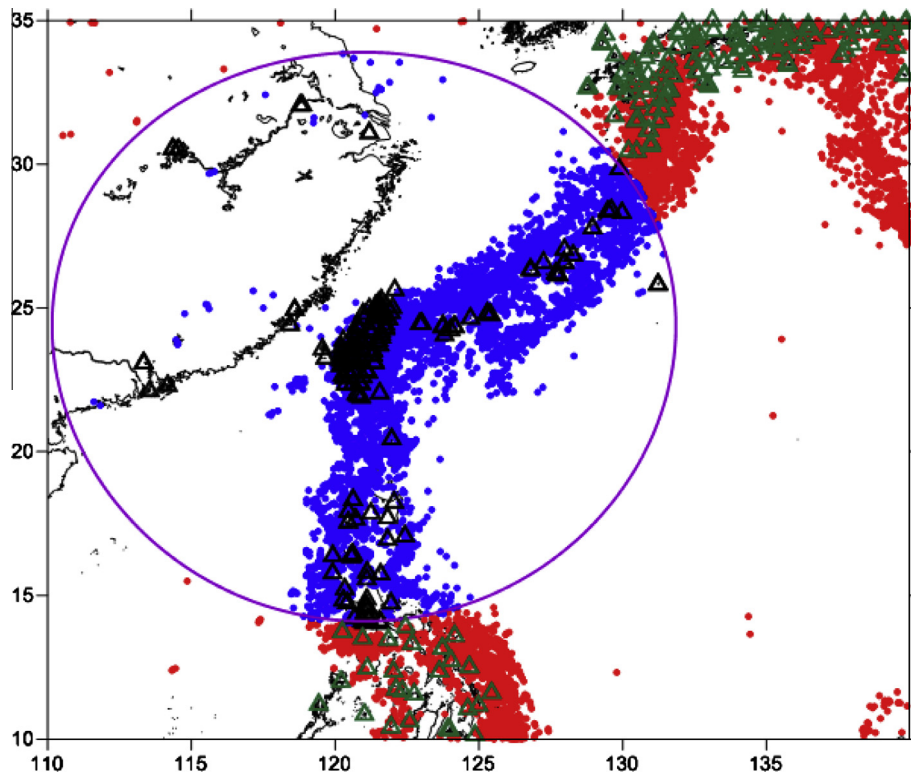


**Fig. 3.** The distribution of data used in this study. Circle depicts the study area. Blue dots are the events recorded by the worldwide stations; red dots are the events recorded by stations in the study area (black triangles), green triangles are the stations outside the study area which recorded the events in the study area. (For interpretation of the references to color in this figure legend, the reader is referred to the web version of this article.)

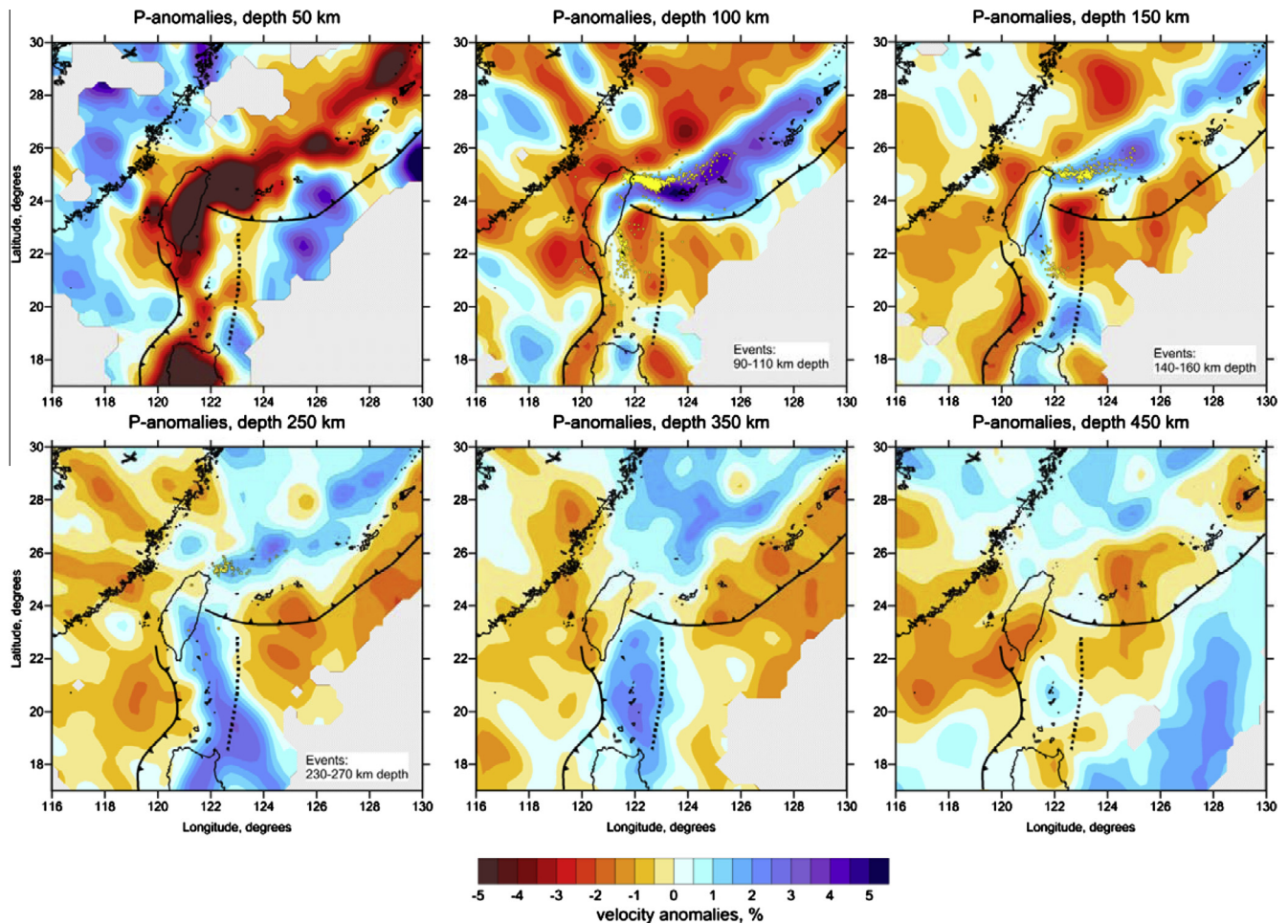


**Fig. 4.** Resulting P-velocity anomalies in horizontal sections. Yellow dots depict the locations of events in corresponding depth intervals, locations of subduction zones and of the Gagua Ridge is the same as in Fig. 1. (For interpretation of the references to color in this figure legend, the reader is referred to the web version of this article.)

depth interval. Both slabs seem to disappear at a depth of 450 km in both the P- and S-models. These slabs can also be observed in the vertical sections in Figs. 6 and 7. The distribution of deep seismicity fits to the upper limit of the slab-related high-velocity anomaly, which serves as one piece of evidence for the reliability of the derived results.

For Section 2 (Fig. 7) representing the Ryukyu subduction, we can clearly see the subduction of the Philippine Sea Plate in the NW direction. The thickness of the slab according to our results remains unchanged at all depths down to  $\sim 400$  km, which is the lowest point of the slab penetration.

For the Luzon arc (Section 1, Fig. 6), the shape of the slab appears to be more complicated. In the upper part of the model, for the S-model, the slab is significantly thinned, whereas for the P-model, it is not observable. For the deeper parts, the slab is clearly traced down to a depth of 400 km. This observation can represent the process of slab detachment by tearing or necking of the subducting lithosphere in the uppermost part. Note that the distribution of deep seismicity in the Benioff zone has its highest density in the area where the slab appears to be thinnest, which is evidence for high stresses in the area of detachment. At the same time, there might be other reasons for such appearance of this subduction segment in the seismic models. As shown by various petrophysical studies (e.g., Hacker et al., 2003) the relationships between seismic velocities, mineralogy, density and water content in the uppermost part of the subduction are rather complex and in some special cases they might lead to lowering the velocity within

slabs. Furthermore, in some cases our ray schemes may not provide optimal resolution for depths of above 100–150 km; thus these gaps might be connected with some artefacts of tomography inversion. On the other hand, as it will be shown later, the synthetic tests with realistic shapes of anomalies demonstrate sufficient resolution for depths of above 120 km and support the robustness of the obtained gap in the slab images.

In both vertical sections we observe a nearly horizontal high-velocity pattern at around 600 km depth which is clearly visible for the P-velocity model. We propose that it might be the trace of stagnant Pacific slab that subducted below the Philippine Sea Plate from the Izu-Bonin and Mariana arcs. Although, the Mariana slab presently appears to be vertically oriented, it was stated in different studies (e.g., Jaxybulatov et al., 2013) that these arcs strongly migrated in the past and it considerably changed the angle of the subducting slab. Similar horizontally oriented stagnant slab is observed beneath Japan (e.g., Zhao, 2004).

For the S-model, the resulting images of the Luzon and Ryukyu slabs and of other features appear to be clearer than in the case of the P-model. For example, in Section 1 between 600 and 800 km along the profile we observe a high S-velocity anomaly which can be interpreted as Eurasian lithosphere. In the P-model, this pattern is not visible. This observation is paradoxical, given the lower quality and the lower amount of the S-data compared to the P-data. However, the higher contrast anomalies in the S-model can be due to the much stronger values of the relevant residuals for the S-times and the higher sensitivity of the S-velocity to

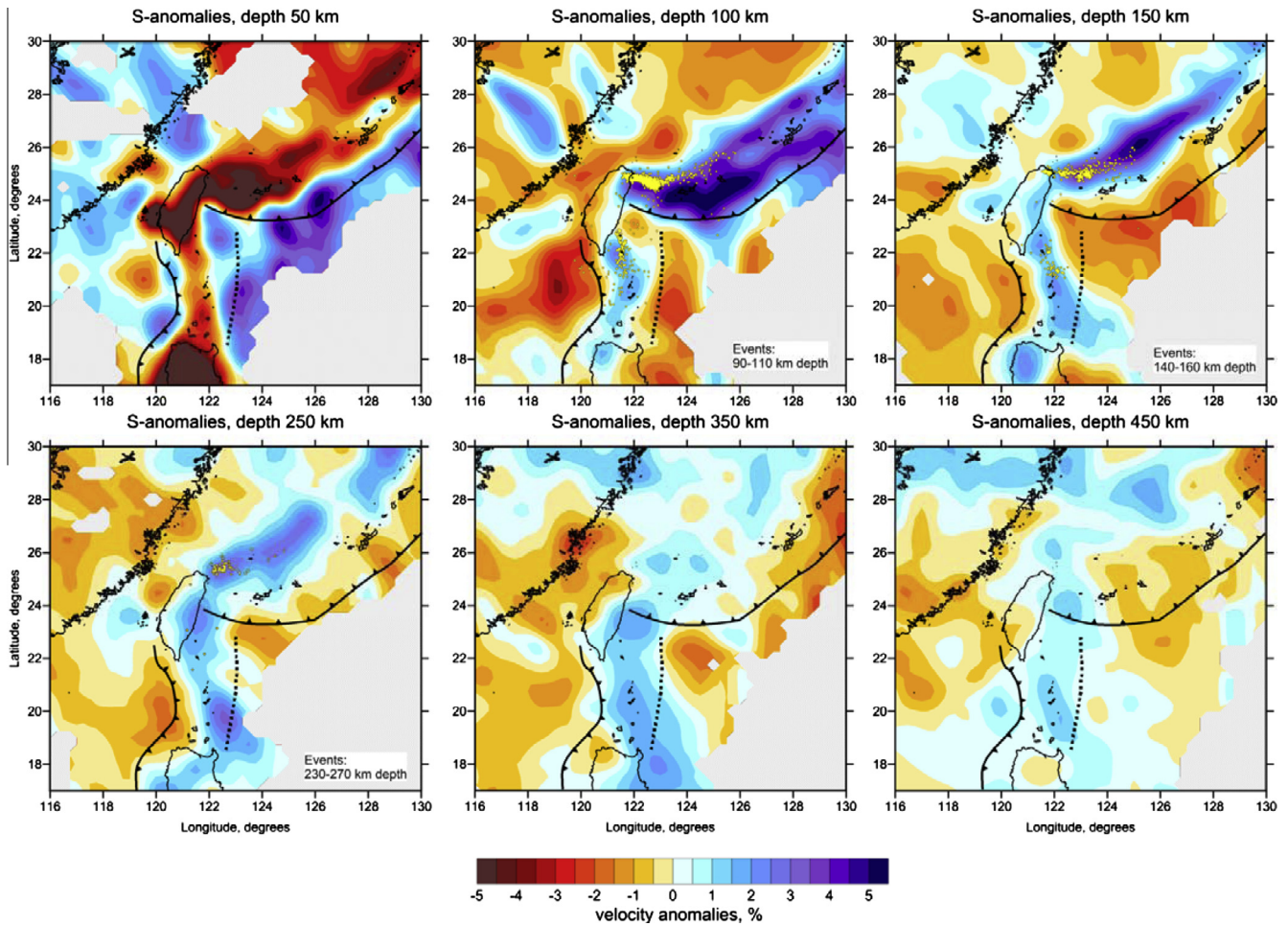


Fig. 5. Same as Fig. 4, but for the S-anomalies.

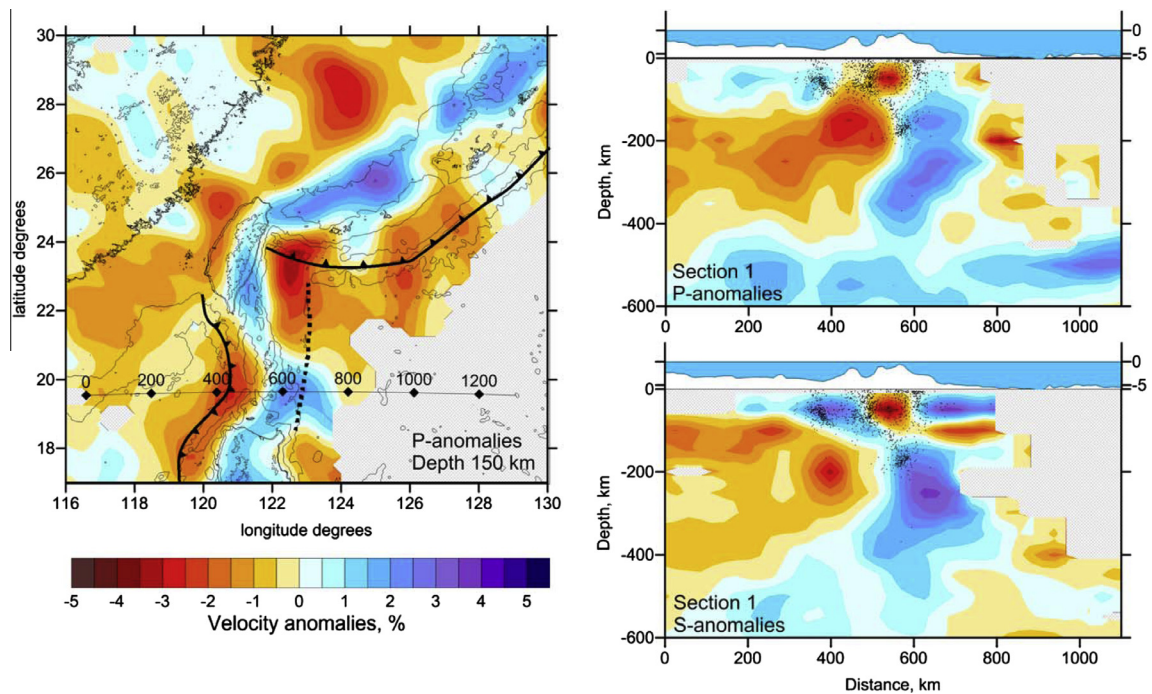


Fig. 6. P and S-velocity anomalies in the vertical section across the Luzon arc (right plots). Relief and bathymetry contour is presented above each section. The locations of the seismicity from the revised ISC catalog at distances of up to 200 km are shown with black dots. To the left is the map view of P-velocity anomalies at 150 km depth with the location of the profile.

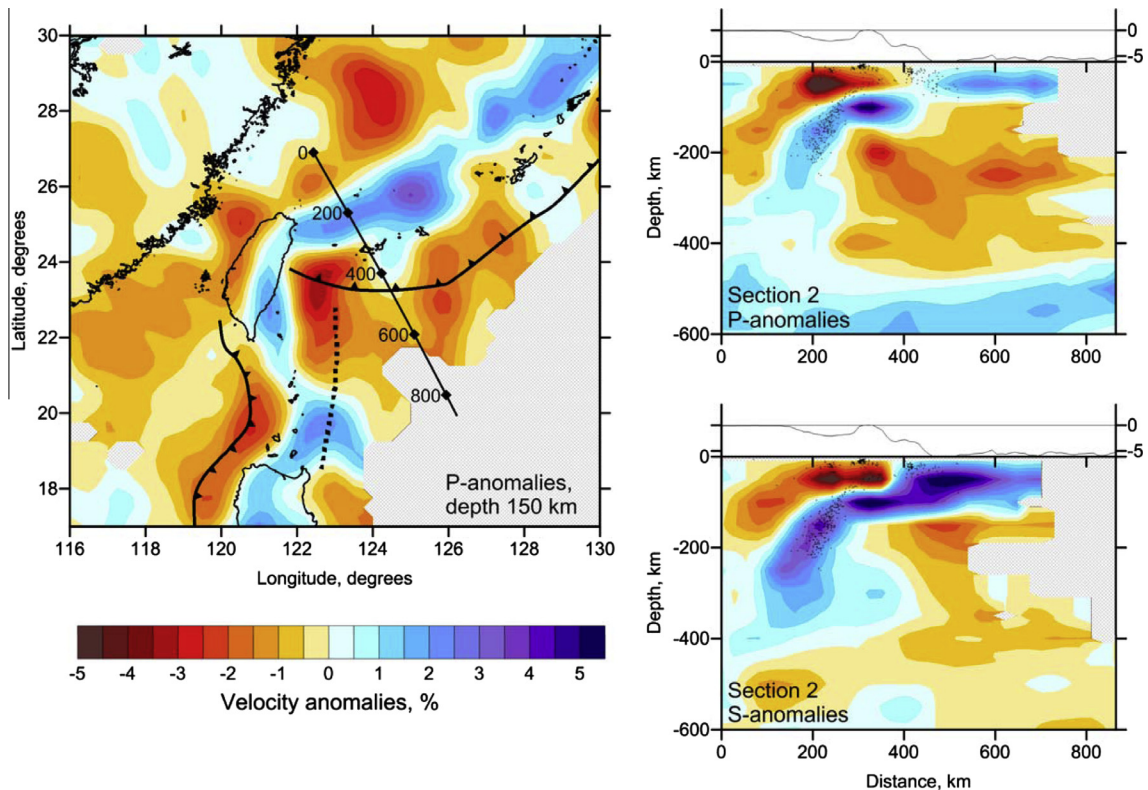


Fig. 7. Same as Fig. 5, but for the vertical section across the Ryukyu Arc. The seismicity is shown for the distances of up to 20 km from the profile.

petrophysical changes in the mantle. It can be estimated based on the existing relationships between petrophysical parameters (e.g., Sobolev and Babeyko, 1994) that a same temperature anomaly in the mantle may result at approximately three times stronger S-residual compared to P-residual. That is why, despite stronger noise in the S-data and their lower amount, in some cases they may provide clearer images for the mantle structures.

To check the resolution capacity of the model, we performed a series of synthetic reconstructions. The synthetic travel times were computed for the realistic source-receiver pairs that were used for the inversion of the observed data. At this step, we used the ray paths computed in the 1D model, as all the calculations were performed in the linearized approach, which seems to be fairly adequate for the expected level of anomalies. The travel times were perturbed with noise having average deviations of 0.4 s and 0.8 s for the P- and S-data, respectively, which enables approximately the same variance reduction as in the case of the observed data inversion.

The results of the traditional checkerboard test are displayed in Fig. 8. The synthetic model consisted of alternating positive and negative anomalies with a size of 200 km  $\times$  200 km in the map view. For increasing depths, the sign of the anomalies changed at every 200 km. The amplitude of the synthetic anomalies was  $\pm 4\%$ . The reconstruction results exhibit reasonable resolution for all depth intervals for the P- and S-models, although for the S-model, we observed a weakening of the amplitude with depth due to the lower amount of the S-data. The P-model generally exhibits higher resolution. The fact that in the case of the observed data, the slab is more clearly observed in the S-model can be explained by the significantly better sensitivity of the S-velocity to the slab-related physical parameters.

The second group of synthetic tests shown in Figs. 9 and 10 was used to determine the reliability of some of the realistic patterns detected in the observed data inversion. The general setup of these tests was similar to that of the checkerboard test, except for the

definition of the synthetic velocity model. In this case, the anomalies were defined in a set of prisms distributed at selected depth intervals. In the map view, the contours of the prism can have rather complex shapes, which represent the realistic distribution of the anomalies. We considered two slightly different models. For the uppermost layer (0–120 km depth), they are identical, whereas for the deeper layer (120–400 km depth), the slab is represented by a continuous anomaly in the 1st model (Fig. 9) and by a set of separated patterns in the 2nd model (Fig. 10). The reconstructed results indicate that these two cases can be clearly distinguished: the gaps in the 2nd model in Fig. 10 are clearly detected in both the P- and S-models. This similarity in the P- and S-models demonstrates that the information on the continuity and on some of the gaps in the slab-related anomalies observed for the observed data results is well resolved and appears to be reliable.

Additional arguments for the robustness of the derived models come from the comparison with results of other tomography studies performed by different authors based on various data sources. In particular, the general configuration of the subducted slabs looks similar to the results of global tomographic modeling (e.g., Bijwaard et al., 1998, Li et al., 2003); although in our models the slab limits appear to be sharper. For the crustal depths our results do not provide good resolution, and the resolution for the shallowest level in our case is poorer compared to some other higher resolution regional models of Taiwan (e.g., Wang et al., 2009). At the same time, for the mantle these models demonstrate very good correlation (see for example section at 250 km depth in Wang et al. (2008) and in Fig. 4 of this paper).

#### 4. Discussion

Based on the results of the regional tomography, we can propose a scenario for the lithosphere development of the Taiwan region, which is schematically displayed in Fig. 11. To elucidate our

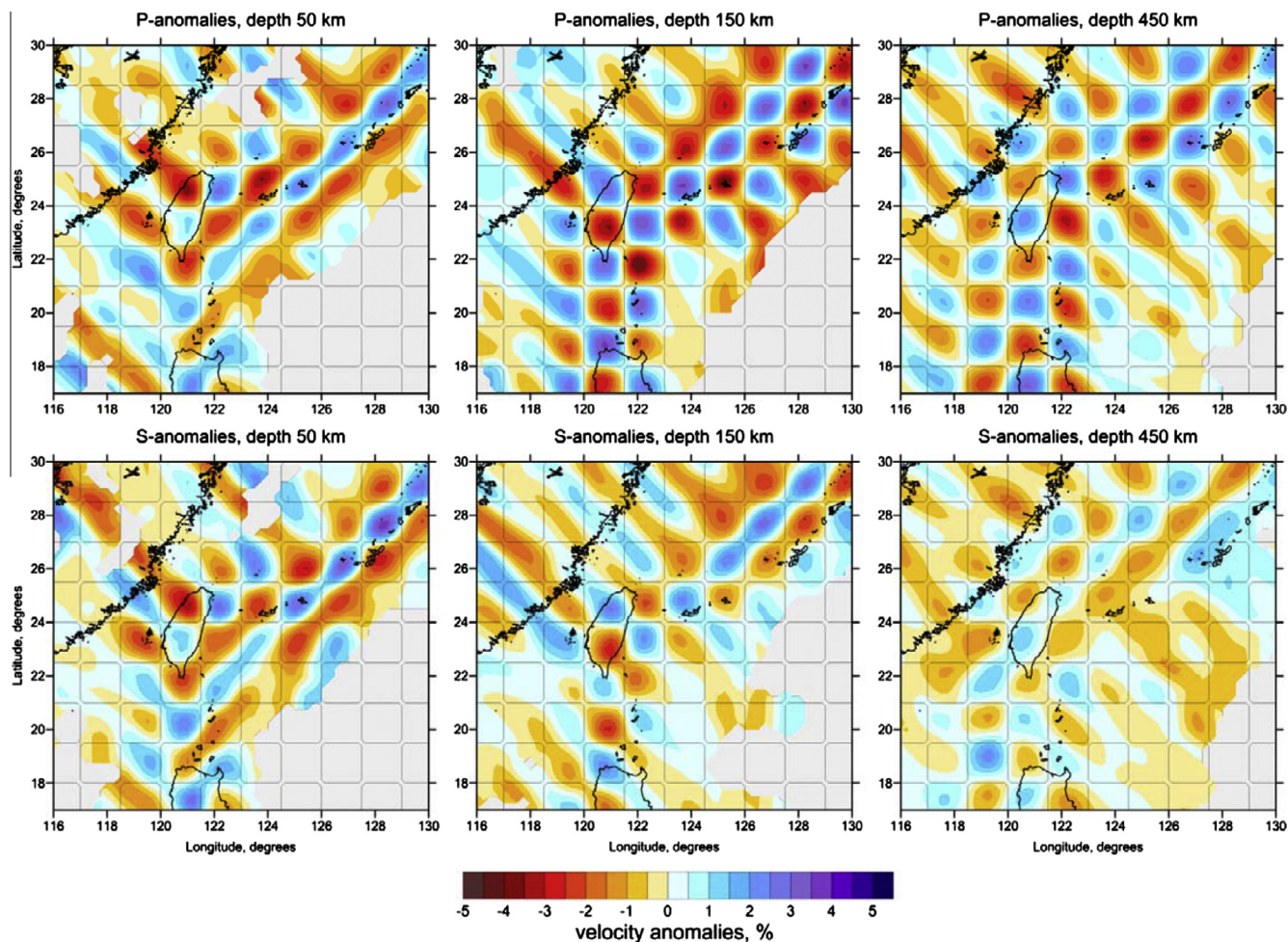


Fig. 8. Results of the checkerboard test for the P- and S-models. The distribution of the initial checkerboard patterns is highlighted with thin lines. Note that the presented depth levels correspond to different signs of anomalies in the synthetic model.

proposed scenario, we prepared a simple “physical” experiment. In Fig. 11A, the two polygons represent the Philippine Sea and the Eurasian plates for the area around Taiwan. The image in Fig. 11A can be copied to a piece of paper and cut to perform further “physical” simulations involving the positioning of the pieces of paper. In Fig. 11B, we present the initial stage of our reconstruction, which corresponds to the age of approximately 5 Ma. At that time, the oceanic plate of the South China Sea was the part of the Eurasian plate subducted below the Luzon arc (segment M–N). The subduction in the Luzon arc occurred due to displacement of the Philippine Sea Plate in the NW direction, and the movement of the Eurasian plate to the opposite direction was much slower. These kinematics led to the displacement of the Luzon arc toward the continental margin of Eurasia. The ocean-ward polarity of subduction, which is the opposite to most other subduction zones, is most likely due to the existence of a large buoyant Luzon Island block of presumably continental nature, which most likely changed the orientation of subduction at previous stages (e.g. Suppe, 1984; Kao et al., 2000).

In the time period corresponding to Fig. 11B, the Philippine Sea Plate subducted almost frontally underneath the Ryukyu arc (segment K–L). We believe that between points N and K, there was a transform fault with a pure shear displacement that was roughly parallel to the displacement of the plate. The existence of such a transform is predicted in most plate reconstructions for this region (e.g., Hall, 1997; Teng, 1990a,b). The movement along this fault led

to the approach of the edge of the Luzon arc (point N) toward the edge of the Ryukyu arc (point K). When these points finally connected (Fig. 11C), the relative displacement between the Eurasian and Philippine Sea Plates was locked, as can be verified by our “physical” experiment using two pieces of paper. Further displacement of the Philippine Sea Plate leads to the tearing and crushing of both pieces of paper near the edges labeled K and N, which might represent the process of collision in the lithosphere near this singular point. Continued displacement of the Philippine Sea Plate led to the deformation of both the Luzon and Ryukyu arcs, as shown in Fig. 11D, which represents the current situation in the Taiwan region. According to this simulation, the Taiwan Island originated from the extreme shortening of the lithosphere at the edge point of two oppositely oriented subduction zones. According to detailed geological analysis of collisional processes in the Taiwan region by Malavielle et al. (2002), the active shortening of the crust here occurred since the last 2 million years that is consistent with our model. Note that according to this scenario, no other conditions, such as the interactions of the buoyant arcs (e.g., Hsu and Sibuet, 1995) and/or the continental lithosphere (e.g., Tang et al., 2002; Teng, 1990a,b), are necessary. The collision can be explained by the relative displacement of the two subduction segments, as demonstrated in Fig. 11.

A similar scenario was proposed by Lallemand et al. (2001) based on a global P-velocity tomography model. At the same time, in their interpretation, the closing the transform fault between the

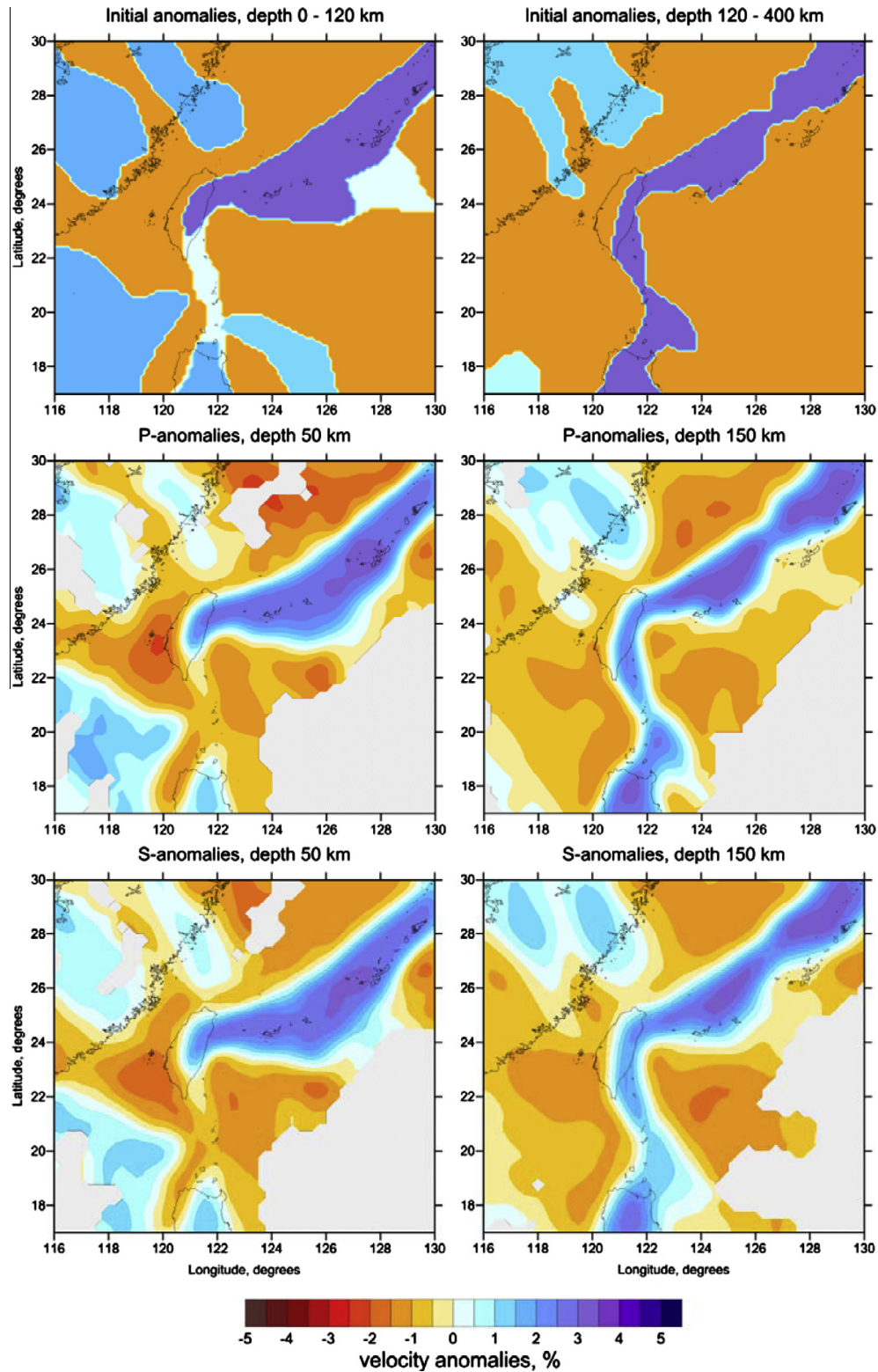


**Fig. 9.** Synthetic test with realistic anomalies – version 1: with continuous slab-related anomalies. The synthetic model (upper row) is defined as polygonal anomalies in the indicated two depth intervals. The lower plots depict the reconstruction of P and S-velocity anomalies at 50 and 150 km depth.

Luzon and Ryukyu arcs occurred about 8 million years ago. We find this hypothesis not plausible. As demonstrated by our “paper modeling”, concentration of strong compression stresses appears immediately after joining two oppositely oriented subduction

zones. Thus we propose that the closing the transform fault occurred not before than 2 million years ago.

The seismic model presented in this paper confirms the collision hypothesis described above. Indeed, the continuous

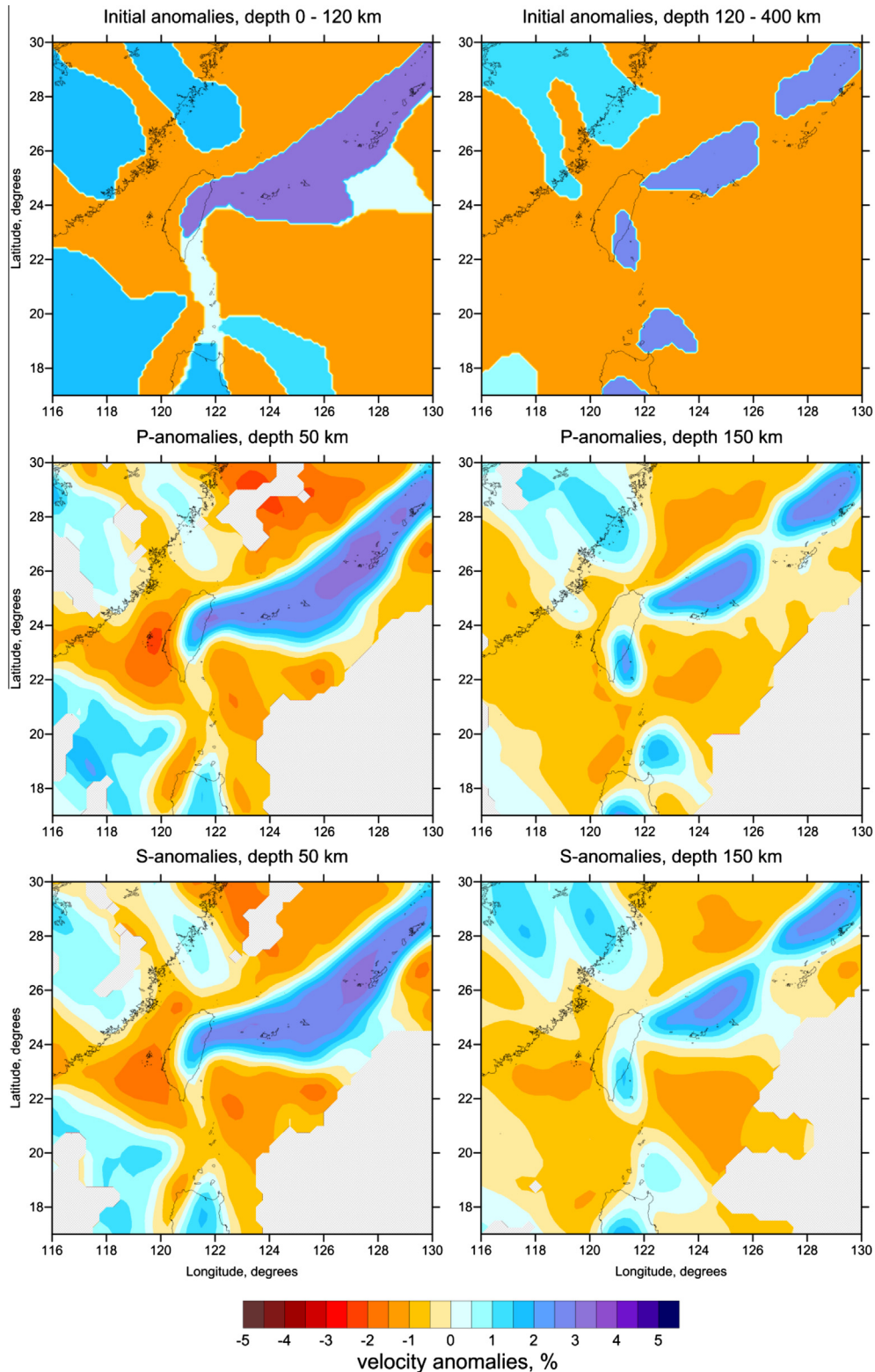


**Fig. 10.** Same as Fig. 7, but the synthetic slab-related anomaly is separated in several parts by small gaps.

slab-related anomaly, which is observed at a depth of 150 km beneath both the Ryukyu and Luzon arcs, demonstrates that the slabs are connected at this depth. The connected slabs indicate that the collision resulting in the origin of the Taiwan Island is not due

to crustal shortening or to the collision of some local buoyant crustal blocks; rather, the collision is caused by the lithosphere collision over a much wider depth interval, as presumed by the scenario shown in Fig. 11. The thinning of the slab related anomaly

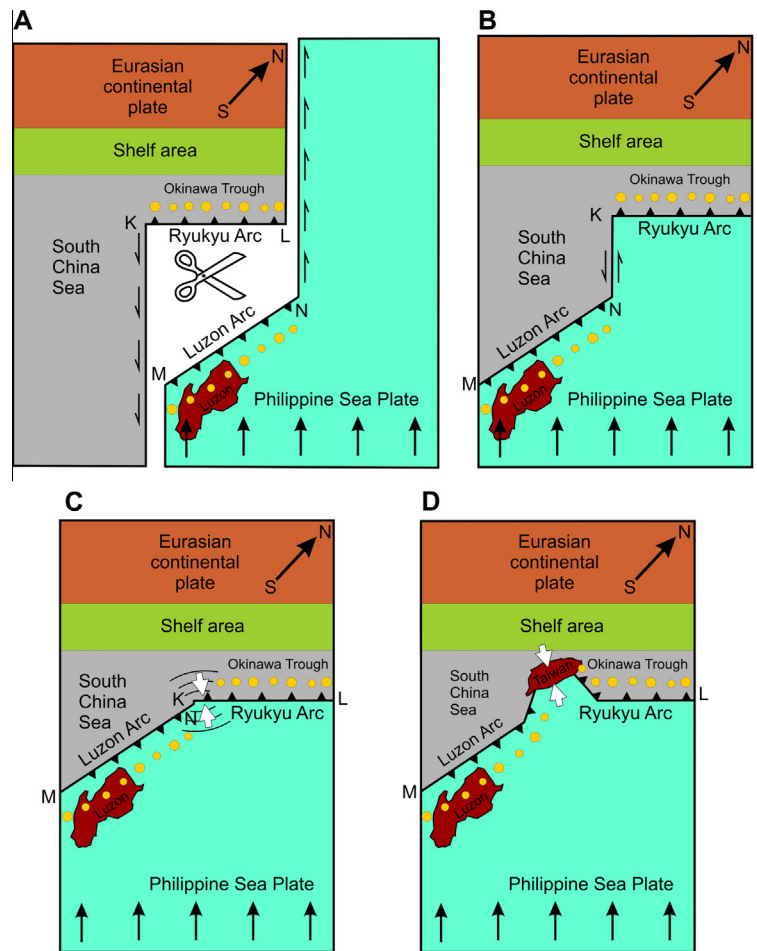


**Fig. 11.** Simplified sketch to explain our story on the plate reconstruction in the study area and on the origin of the Taiwan Island. A represent the contours of two major plated which can be cut and used for simple simulations of plate movements. B–D depict three stages of the plate reconstructions. Yellow circles schematically depict the locations of arc volcanoes. The location of major shortening at the edges of the subduction zones is indicated by white arrows. See more details in the text. (For interpretation of the references to color in this figure legend, the reader is referred to the web version of this article.)

at 2shallow depths for Section 1 across the Luzon arc possibly indicates the tearing of the slab due to the interaction of two oppositely oriented subduction zones.

## 5. Conclusions

In this study, we have performed a regional-scale tomographic inversion and obtained clear images of two subducting slabs beneath the Ryukyu and Luzon arcs. In general, our model agrees with most of the previous global and regional tomographic models. The correspondence of several models obtained using different approaches with the data is an important argument for the reliability of the derived structures. A high correlation between the P- and S-velocity anomalies is validation of the robustness of the slab reconstructions.

In our case, we paid particular attention to determining whether the Eurasian and Philippine Sea slabs touch each other beneath Taiwan. We conclude that at depths ranging from 100 to 200 km, these slabs exhibit a united anomaly, which provides evidence for the collision of these slabs. Simple simulations with paper models indicate that at the edge of the collision of two oppositely oriented subduction zones, very strong stresses and deformations can occur in a localized zone. We believe that these deformations caused strong crustal shortening and resulted in the origin of the Taiwan Island. Of particular importance is the fact

that the shortening can occur from the interaction of two subduction zones alone and does not require any other preconditions, such as the existence of arcs or buoyant continental blocks, as presumed by some of the other hypotheses for the origin of the Taiwan Island.

## Acknowledgements

This study was supported by the Joint Research Project of the Siberian Branch of RAS and the National Science Council of Taiwan.

## References

- Bijwaard, H., Spakman, W., Engdahl, E.R., 1998. Closing the gap between regional and global travel time tomography. *Journal of Geophysical Research* 103, 30055–30078.
- Bird, P., 2003. An updated digital model of plate boundaries. *Geochemistry Geophysics Geosystems* 4 (3), 1027. <http://dx.doi.org/10.1029/2001GC000252>.
- Bonvalot, S., Balmino, G., Briais, A., Kuhn, M., Peyrefitte, A., Vales N., Biancale, R., Gabalda, G., Moreaux, G., Reinquin, F., Sarrailh, M., 2012. World Gravity Map, 1:50000000 map, Eds.: BGI-CGMW-CNES-IRD, Paris.
- Chemenda, A.I., Yang, R.K., Stephan, J.F., Konstantinovskaya, E.A., Ivanov, G.M., 2001. New results from physical modelling of arc-continent collision in Taiwan: evolutionary model. *Tectonophysics* 333, 159–178.
- Hacker, B.R., Abers, G.A., Peacock, S.M., 2003. Subduction factory, 1. Theoretical mineralogy, densities, seismic wave speeds, and H<sub>2</sub>O contents. *J. Geophys. Res.*, 108(B1), 2029, doi: <http://dx.doi.org/10.1029/2001JB001127>.
- Hall, R., 1997. Cenozoic plate tectonic reconstructions of SE Asia. In: Fraser, A., Matthews, S.J., Murphy, R.W. (Eds.), *Petroleum Geology of SE Asia*. Geological Society of London Special Publication, 126, 11–23.

- Hsu, S.K., 2001. Subduction/collision complexities in the Taiwan-Ryukyu junction area: tectonics of the Northwestern corner of the Philippine Sea plate. *Journal of Terrestrial, Atmospheric and Ocean Sciences* 12, 209–230.
- Hsu, S.K., Sibuet, J.C., 1995. Is Taiwan the result of arc-continent or arc-arc collision? *Earth and Planetary Science Letters* 136, 315–324.
- International Seismological Centre, 2001. *Bulletin Disks 1–9* [CD-ROM]. International. Seis. Cent, Thatcham, United Kingdom.
- Jaxybulatov, K., Koulakov, I., Dobretsov, N.L., 2013. Segmentation of the Izu-Bonin and Mariana plates based on the analysis of the Benioff seismicity distribution and regional tomography results. *Solid Earth* 4, 59–73. <http://dx.doi.org/10.5194/se-4-59-2013>.
- Kao, H., Huang, G.C., Liu, C.S., 2000. Transition from oblique subduction to collision in the northern Luzon arc-Taiwan region: Constraints from bathymetry and seismic observations. *Journal of Geophysical Research: Solid, Earth* (1978–2012) 105 (B2), 3059–3079.
- Kim, K.H., Chiu, J.M., Pujol, J., Chen, K.C., Huang, B.S., Yeh, Y.H., Shen, P., 2005. Three-dimensional Vp and Vs structural model associated with the active subduction and collision tectonics in the Taiwan region. *Geophysical Journal International* 162, 204–220.
- Koulakov, I., 2011. High-frequency P and S velocity anomalies in the upper mantle beneath Asia from inversion of worldwide traveltime data. *Journal of Geophysical Research* 116, B04301. <http://dx.doi.org/10.1029/2010JB007938>.
- Koulakov, I., Sobolev, S.V., 2006. A tomographic image of Indian lithosphere break-off beneath the Pamir Hindukush Region. *Geophysical Journal International* 164, 425–440.
- Koulakov, I., Tychkov, S., Bushenkova, N., Vasilevskiy, A., 2002. Structure and dynamics of the upper mantle beneath the Alpine-Himalayan orogenic belt from teleseismic tomography. *Tectonophysics* 358, 77–96.
- Koulakov, I., Kaban, M.K., Tesauro, M., Cloetingh, S., 2009. P and S velocity anomalies in the upper mantle beneath Europe from tomographic inversion of ISC data. *Geophysical Journal International* 179 (1), 345–366. <http://dx.doi.org/10.1111/j.1365-246X.2009.04279.x>.
- Koulakov, I., Dobretsov, N.L., Bushenkova, N.A., Yakovlev, A.V., 2011. Slab shape in subduction zones beneath the Kurile–Kamchatka and Aleutian arcs based on regional tomography results. *Russian Geology and Geophysics* 52, 650–667.
- Ku, C.-Y., Hsu, S.-K., 2009. Crustal structure and deformation at the northern Manila Trench between Taiwan and Luzon islands. *Tectonophysics* 466, 229–240.
- Lallemand, S., Font, Y., Bijwaard, H., Kao, H., 2001. New insights on 3-D plates interaction near Taiwan from tomography and tectonic implications. *Tectonophysics* 335, 229–253.
- Li, C., van der Hilst, R.D., Engdahl, E.R., Burdick, S., 2008. A new global model for P wave speed variations in Earth's mantle. *Geochemistry, Geophysics Geosystems* 9 (5).
- Lin, C.H., 2000. Thermal modeling of continental subduction and exhumation constrained by heat flow and seismicity in Taiwan. *Tectonophysics* 324, 189–201.
- Lin, C.H., 2002. Active continental subduction and crustal exhumation: the Taiwan orogeny. *Terra Nova* 14, 281–287.
- Lin, J.Y., Sibuet, J.C., Lee, C.S., Hsu, S.K., Klingelhoefer, F., 2007. Origin of the southern Okinawa Trough volcanism from detailed seismic tomography. *Journal of Geophysical Research* 112, B08308. <http://dx.doi.org/10.1029/2006JB004703>.
- Ma, K.F., Wang, J.H., Zhao, D., 1996. Three-dimensional seismic velocity structure of the crust and uppermost mantle beneath Taiwan. *Journal of Physics of the Earth* 44, 85–105.
- Malavieille, J., Lallemand, S.E., Dominguez, S., Deschamps, A., 2002. Arc-continent collision in Taiwan: new marine observations and tectonic evolution. *Geological Society of America, Special Paper* 358, 187–211.
- McIntosh, K., Nakamura, Y., Wang, T.K., Shih, R.C., Chen, A.T., Liu, C.S., 2005. Crustal-scale seismic profiles across Taiwan and the western Philippine Sea. *Tectonophysics* 401, 23–54.
- Nakamura, Y., McIntosh, K., Chen, A.T., 1998. Preliminary results of a large offset seismic survey west of Hengchun Peninsula, southern Taiwan. *Journal of Terrestrial, Atmospheric and Ocean Sciences* 9, 395–408.
- Nolet, G., 1987. Seismic wave propagation and seismic tomography. In: G.Nolet (Ed.), *Seismic Tomography*, Reidel, Dordrecht, 1–23.
- Paige, C.C., Saunders, M.A., 1982. LSQR: An algorithm for sparse linear equations and sparse least squares. *ACM Transactions on Mathematical Software* 8, 43–71.
- Rau, R.-J., Wu, F.T., 1995. Tomographic imaging of lithospheric structures under Taiwan. *Earth and Planetary Science Letters* 133, 517–532.
- Roecker, S.W., Yeh, Y.H., Tsai, Y.B., 1987. Three-dimensional P and S wave velocity structures beneath Taiwan; deep structure beneath an arc-continent collision. *Journal of Geophysical Research* 92, 10547–10570.
- Shin, T.C., Chen, Y.L., 1988. Study on the earthquake location of 3-D velocity structure in the Taiwan area. *Meteorological Bulletin* 42, 135–169.
- Sobolev, S.V., Babeyko, A.Yu., 1994. Modeling of mineralogical composition, density and elastic wave velocities in anhydrous magmatic rocks. *Surveys in Geophysics* 15, 515–544.
- Suppe, J., 1981. Mechanics of mountain building and metamorphism in Taiwan. *Memoir of the Geological Society of China* 4, 67–89.
- Suppe, J., 1984. Kinematics of arc-continent collision, flipping of subduction, and back-arc spreading near Taiwan. *Memoir of the Geological Society of China* 6, 21–33.
- Tang, J.C., Chemenda, A.I., Chery, J., Lallemand, S., Hassani, R., 2002. Compressional subduction regime and arc-continent collision: numerical modeling. *Geological Society of America, Special Publication* 358, 177–186.
- Teng, L.S., 1990a. Geotectonic evolution of late Cenozoic arc-continent collision in Taiwan. *Tectonophysics* 183, 57–76.
- Teng, L.S., 1990. Geotectonic evolution of late Cenozoic arc-continent collision in Taiwan. In: Angelier, J. (Ed.), *Geodynamic Evolution of the Eastern Eurasian Margin*. *Tectonophysics* 183, 57–76.
- Wang, Z., Zhao, D., Wang, J., Kao, H., 2006. Tomographic evidence for the Eurasian lithosphere subducting beneath south Taiwan. *Geophysical Research Letters* 33, L18306. <http://dx.doi.org/10.1029/2006GL027166>.
- Wang, Z., Huang, R., Huang, J., He, Z., 2008. P-wave velocity and gradient images beneath the Okinawa Trough. *Tectonophysics* 455 (1), 1–13.
- Wang, Z., Fukao, Y., Zhao, D., Kodaira, S., Mishra, O.P., Yamada, A., 2009. Structural heterogeneities in the crust and upper mantle beneath Taiwan. *Tectonophysics* 476 (3), 460.
- Wu, F.T., Rau, R.J., Salzberg, D., 1997. Taiwan orogeny: thin-skinned or lithospheric collision? *Tectonophysics* 274, 191–220.
- Wu, Y.M., Chang, C.H., Zhao, L., Shyu, J.B.H., Chen, Y.G., Sieh, K., Avouac, J.P., 2007. Seismic tomography of Taiwan: improved constraints from a dense network of strong-motion stations. *Journal of Geophysical Research* 112, B08312. <http://dx.doi.org/10.1029/2007JB004983>.
- Yu, S.B., Chen, H.Y., Kuo, L.C., Lallemand, S.E., Tsien, H.H., 1997. Velocity field of GPS stations in the Taiwan area. *Tectonophysics* 274, 41–59.
- Zhao, D., 2004. Global tomographic images of mantle plumes and subducting slabs: insight into deep Earth dynamics. *Physics of the Earth and Planetary Interiors* 146, 3–34.